Molecular Physics, 2015
Vol. 113, No. 1, 28–35, http://dx.doi.org/10.1080/00268976.2014.941024

RESEARCH ARTICLE

Chemical potentials and phase equilibria of Lennard-Jones chain fluids

Patsy V. Ramírez-González[a], Sergio E. Quiñones-Cisneros[b,*] and Ulrich K. Deiters[c]

[a]*Departamento de Ingeniería Química, Facultad de Química, Universidad Nacional Autónoma de México, México D.F., Mexico;* [b]*Instituto de Investigaciones en Materiales, Universidad Nacional Autónoma de México, México D.F., Mexico;* [c]*Institute of Physical Chemistry, University of Cologne, Cologne, Germany*

(*Received 13 November 2013; accepted 24 June 2014*)

Computer simulations (molecular dynamics) were performed for ensembles of flexible tangent Lennard-Jones chains consisting of n sites ($n = 1$, 2, 4, 8, and 16). From these simulations, the orthobaric liquid and vapour densities were calculated not only with the traditional method of simulating a liquid film in coexistence with vapour, but also using the rigorous thermodynamic condition of satisfying the chemical potential equality between the phases in equilibrium. The agreement with literature data, as far as such exist, is excellent.

Keywords: Lennard-Jones chains; orthobaric density; chemical potential; computer simulation; molecular dynamics

1. Introduction

Over the previous decades, many publications reported the properties of the Lennard-Jones (LJ) fluid; the well-known textbook of Hirschfelder, Curtiss, and Bird [1] already cites many publications, where properties were calculated from integral equations, cluster integrals, or similar tools. The LJ fluid has been studied extensively with computer simulation methods (molecular dynamics (MD) or Monte Carlo techniques) as well as the statistical–mechanical methods like the perturbation theory. The amount and the quality of the thermophysical properties obtained by these methods have allowed for the development of reference equations of state (EOSs) for the LJ fluid [2–4], from which the equation of Mecke *et al*. [5] is probably the most recent one.

For the LJ dimer fluid, the data situation is also quite good, and consequently an EOS could also be constructed [6]. Furthermore, computer simulations have also been reported for flexible tangent LJ chain fluids [7,8]. The number of publications dealing with this class of fluids, however, is much smaller than for LJ monomers and dimers. The properties obtained from these simulations are mostly pVT and the phase equilibrium; again, an EOS for LJ chains was also proposed [7].

However, thermophysical properties of LJ chain molecules have not been explored as thoroughly as for LJ monomers and dimers, at least not for the whole fluid region (low to high densities). We have therefore undertaken computer simulations of flexible tangent LJ chain fluids with chain lengths between 1 and 16 and have determined pVT data, chemical potentials, and vapour–liquid phase equilibria.

2. Theory

2.1. Interaction potentials

In this work, we consider flexible molecules consisting of n tangent spherical sites, where n is 1, 2, 4, 8, or 16. The full site–site LJ interaction potential is

$$u_{\mathrm{LJ}}(r) = 4\varepsilon\left[\left(\frac{\sigma}{r}\right)^{12} - \left(\frac{\sigma}{r}\right)^{6}\right], \tag{1}$$

where ε is the energy constant (or well depth), σ is the diameter of a site, and r is the site–site separation. In this work, we use the spherically truncated and shifted LJ potential [9]:

$$u_{\mathrm{STS}}(r) = \begin{cases} u_{\mathrm{LJ}}(r) - u_{\mathrm{LJ}}(r_{\mathrm{cut-off}}) & r < r_{\mathrm{cut-off}} \\ 0 & r \geq r_{\mathrm{cut-off}} \end{cases}, \tag{2}$$

where $r_{\mathrm{cut\text{-}off}}$ is the cut-off distance. Thus, the spherically truncated force is given by

$$F(r) = \begin{cases} -\frac{du_{\mathrm{LJ}}(r)}{dr} & r < r_{\mathrm{cut-off}} \\ 0 & r \geq r_{\mathrm{cut-off}} \end{cases}. \tag{3}$$

The calculations were carried out using the LJ parameters of argon, $\varepsilon/k_{\mathrm{B}} = 119.8$ K and $\sigma = 0.3405$ nm, where k_{B} is the Boltzmann constant. Throughout this work, reduced (dimensionless) properties are used: $t^* = \frac{t}{\sigma}\sqrt{\frac{\varepsilon}{m_{\mathrm{p}}}}$, $T^* = \frac{k_{\mathrm{B}}T}{\varepsilon}$, $\rho^* = \sigma^3\rho$, $p^* = \frac{p\sigma^3}{\varepsilon}$, $\mu^* = \frac{\mu}{\varepsilon}$, where t is the time, m_{p} is the mass of a particle or 'atom', T is the temperature, ρ is the atomic number density, p is the pressure, and μ is the chemical potential.

* Corresponding author. Email: seqc@unam.mx

A chain is defined as a molecule made of n atoms joined by strong harmonic bonds described by a simple spring-type potential [7]:

$$u_{\text{bond}} = -\frac{1}{2}k\,(r-\sigma)^2\,. \tag{4}$$

We used a value of $3000\,\varepsilon/\sigma^2$ for the spring constant k, as also proposed by Johnson *et al*. [7]. No bond angle deformation or torsion potentials are used, i.e., the chain molecules studied in this work are fully flexible.

2.2. Simulation details

The simulations reported here were based on the molecular dynamics method, using an NVT ensemble. The temperature was kept constant by velocity scaling. The simulation code was developed by the authors.

The reduced time step was $\Delta t^* = 0.0025$ and the cut-off distance was set to 5.5σ. The number of molecules were 1000 for $n = 1$, 800 (1600 atoms) for $n = 2$, 400 (1600 atoms) for $n = 4$, 300 (2400 atoms) for $n = 8$, and 200 (3200 atoms) for $n = 16$. A Verlet [10] algorithm and periodic boundary conditions were used. For all properties, standard deviations were computed in order to obtain the statistical errors.

At the beginning of a simulation run, the molecules were placed into an expanded simulation box; then the box was compressed to the desired density. In contrast to the common practice of starting from a crystalline initial configuration, this method does not require designing a crystal structure (for some non-spherical molecules not a trivial task) and eliminates the danger that the order of the crystal affects the structure of the fluid. Equilibration was observed to be rapid even for dense states; usually around 1×10^6 MD steps were used for this stage, and 5×10^6 MD steps were used for the production stage.

2.3. Phase equilibrium

Phase equilibria were determined directly by simulating a liquid film in coexistence with vapour [11,12]. In order to obtain equilibrated films of sufficient thickness, first the liquid was equilibrated in a simulation box with one side five to eight times longer than the other two sides ($L_x = L_y = 11\sigma$ and $L_z = 55\sigma$–88σ). Then, forces of opposing direction were applied on each side of the box (see Figure 1(a)). These forces acted like a gravitational field forming a liquid film at the centre of the box. Once the film had been formed, the gravity was turned off, and the particles began to evaporate until equilibrium was reached (see Figure 1(b)). If necessary, a correction to the centre of mass was made to avoid any displacement of the film. After equilibrium had been reached, a density profile was constructed (Figure 2). For this, the simulation box was divided into 200 equal slices and the average over time of the number of particles inside each section was estimated.

The orthobaric bulk liquid and vapour densities, ρ_{liq} and ρ_{vap}, respectively, were first obtained by fitting a

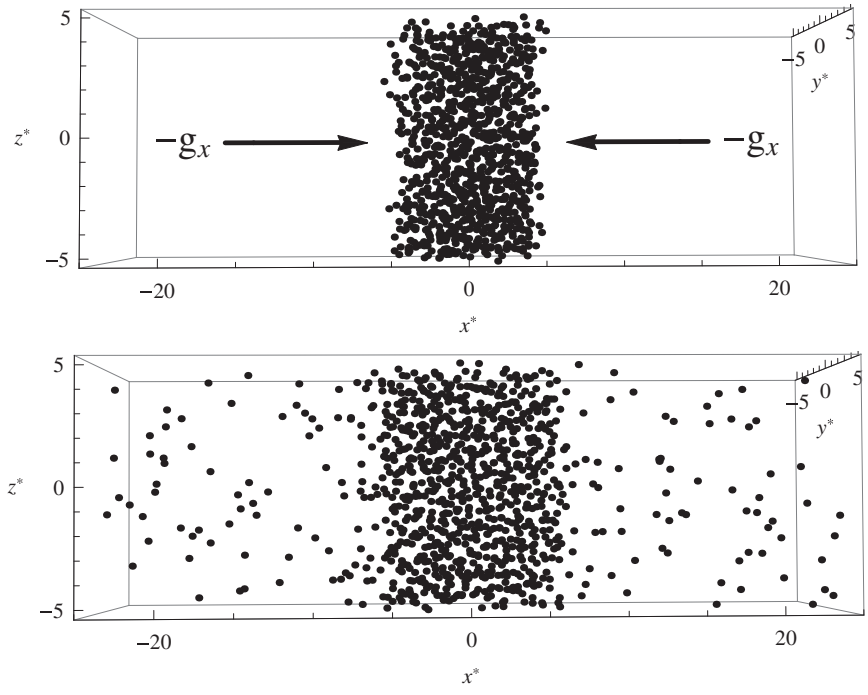

Figure 1. (a) Formation of a liquid film and (b) liquid and vapour in coexistence for $T^* = 1$.

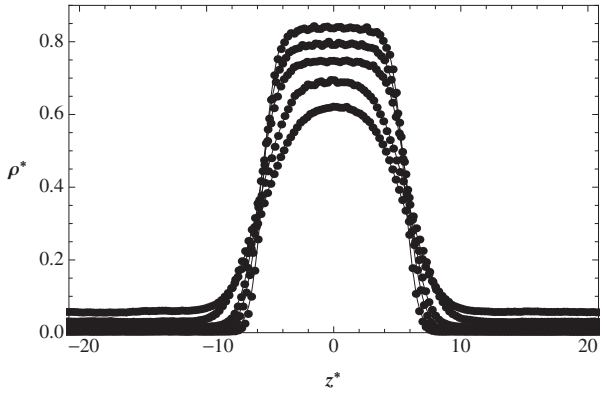

Figure 2. Determination of the equilibrium densities from a density profile for $n = 1$. •: simulation, —: fitted hyperbolic-tangent profile, Equation (3). From bottom to top: $T^* = 1.1$, $T^* = 1$, $T^* = 0.9$, $T^* = 0.8$, and $T^* = 0.7$.

hyperbolic-tangent profile to the local density data [13],

$$\rho(z) = \frac{1}{2}(\rho_{\text{liq}} + \rho_{\text{vap}}) - \frac{1}{2}(\rho_{\text{liq}} - \rho_{\text{vap}}) \tanh\left(\frac{2z}{d}\right), \tag{5}$$

where z is the coordinate perpendicular to a vapour–liquid interface centred at the origin and d is the interfacial thickness.

2.4. Chemical potential

The chemical potential is an important thermodynamic quantity that controls not only the diffusion of the species, but also chemical reactions. One practical way to calculate chemical potentials is Widom's method [14], according to which a 'ghost' molecule is inserted randomly into a system of n atoms; the resulting change of the internal energy, ΔU, is recorded. The residual chemical potential is obtained as [15]

$$\mu_{\text{res}} = -k_B T \ln\left\langle \exp\left(-\frac{\Delta U}{k_B T}\right)\right\rangle, \tag{6}$$

where μ_{res} is the residual chemical potential. In order to avoid numerical overflow conditions, insertion attempts were aborted when the distance of the inserted atom from any other atom becomes less than 0.8σ.

For chains, we try to insert the entire molecule at once. This is achieved by inserting the first atom randomly; next, another atom is attached to the first one, and a check for an overlap with all other atoms in the system is made (if there is one, the insertion attempt of this chain is aborted; otherwise, the energy needed for this insertion is recorded). This procedure is repeated until the complete chain has been inserted. Then the sum of all single-atom insertion energies is used in Equation (6).

For the calculation of the total chemical potential, the ideal-gas chemical potential [16] is also required,

$$\mu_{\text{id}} = k_{\text{B}} T \ln\left(N\lambda^3/V\right), \tag{7}$$

where $\lambda = \frac{h}{\sqrt{2\pi m_{\text{p}} k_{\text{B}} T}}$ is the de Broglie wavelength and h is the Planck constant.

The insertion method outlined above becomes inefficient for long-chain molecules at high densities, because the probability of finding vacancies for 8 or 16 atoms gets very small and a large number of insertion attempts have to be made to obtain significant contributions to the average Boltzmann factor in Equation (6). To overcome this difficulty, it is possible to devise sequential insertion schemes. For this work, however, a more efficient method is used [17]. According to classical thermodynamics, the residual chemical potential of a pure fluid can be obtained by

$$\mu_{\text{res}} = -\int_{\infty}^{V_m} p_{\text{res}} dV_m + pV_m - RT. \tag{8}$$

Using the reduced density as integration variable and switching to reduced quantities yields

$$\mu^*_{\text{res}} = m\int_0^{\rho^*} \frac{p^*_{\text{res}}}{\rho^2}\, d\rho^* + \frac{m p^*_{\text{res}}}{\rho^*}, \tag{9}$$

where

$$p^*_{\text{res}} = p^* - \frac{\rho^* T^*}{m} \tag{10}$$

denotes the reduced residual pressure. To compute μ^*_{res} values, we constructed smoothing natural cubic spline functions [18] through $p^*(\rho^*)$ data obtained in this work and integrated these analytically.

The evaluation of the pressure in a molecular simulation involves an ensemble average of the pairwise interactions that can be written explicitly in the usual virial form as [19]

$$p = \langle \rho k_{\text{B}} T\rangle + \left\langle \frac{1}{3V}\sum_i \sum_{j<i} \mathbf{r}_{ij}\cdot\mathbf{f}_{ij}\right\rangle, \tag{11}$$

where $\rho = N/V$ is the number density, $\mathbf{r}_{ij}$ is the intermolecular vector between a pair, and $\mathbf{f}_{ij}$ denotes the forces exerted on atom i by atom j. The first term on the right-hand side of Equation (11) is the kinetic (ideal-gas) contribution and the second term represents the residual contribution arising from the interactions.

3. Results

3.1. Phase equilibrium results

In Figure 1(a), we can observe the formation of the liquid film with the help of an external force (gravity) for $m = 1$ and in Figure 1(b), we can observe the coexistence of the liquid with the vapour. In Figure 2, the density profile is presented for different temperatures for $n = 1$, with the profiles fitted with Equation (5).

If the same method is applied for different temperatures, a T–ρ diagram can be constructed. Figure 3 shows a comparison of our results with the reference data reported by Trokhymchuk and Alejandre [9] for the same cut-off distance.

The ρ_{liq} and ρ_{vap} of every system ($n = 1, 2, 4, 8$, and 16) were calculated for several temperatures. Figure 4 shows the vapour–liquid equilibrium diagram for different number of atoms in the chain compared with reference data reported by MacDowell and Blas [20]. As expected, the phase envelope shifts to lower temperatures with increasing chain length.

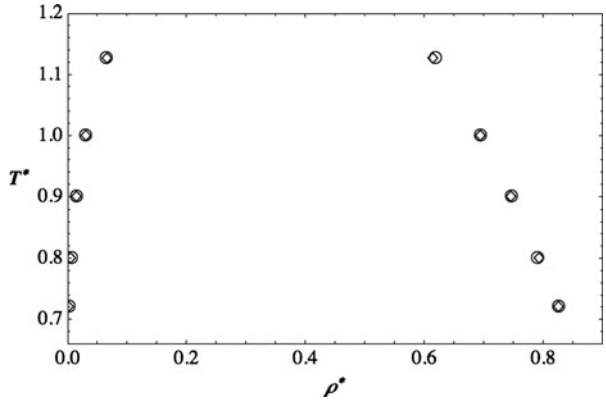

Figure 3. Reduced orthobaric densities as functions of the reduced temperature for $n = 1$. ○: MD simulation (this work), □: Trokhymchuk and Alejandre [9].

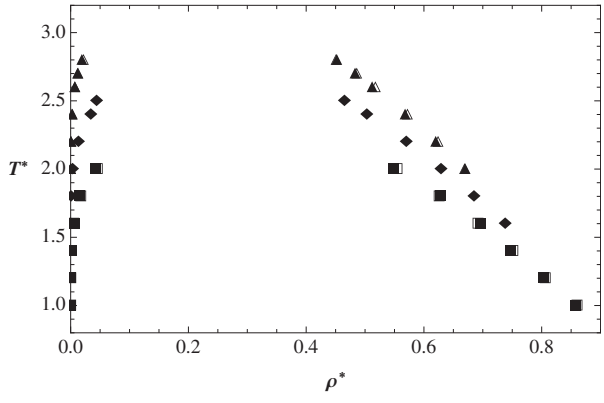

Figure 4. Vapour–liquid equilibrium (temperature vs. density) for chains of different lengths: ■: $n = 4$, ♦: $n = 8$, and ▲: $n = 16$ (this work) and □: $n = 4$, ◇: $n = 8$, and △: $n = 16$ (data from MacDowell and Blas [20]).

Table 1. Reduced orthobaric densities for flexible Lennard-Jones chains of length n.

T^*	ρ^*_{liq}	ρ^*_{vap}	P^*
$n = 1$			
0.7	0.826(3)	0.0021(3)	0.00096(5)
0.8	0.790(3)	0.0063(2)	0.0048(4)
0.9	0.747(2)	0.0152(5)	0.0123(5)
1	0.694(5)	0.0303(3)	0.0258(5)
1.127	0.618(5)	0.0646(6)	0.0571(4)
$n = 2$			
1	0.824(3)	0.0017(2)	0.00063(5)
1.2	0.755(4)	0.0081(3)	0.0042(6)
1.3	0.716(3)	0.015(4)	0.0084(7)
1.4	0.677(2)	0.026(3)	0.0153(4)
1.5	0.628(1)	0.0488(2)	0.0255(5)
1.6	0.572(4)	0.082(1)	0.0397(7)
$n = 4$			
1	0.857(5)	0.00004(2)	0.0000008(5)
1.2	0.804(4)	0.0005(3)	0.000028(5)
1.4	0.747(3)	0.0015(2)	0.0003(6)
1.6	0.696(3)	0.006(1)	0.0016(5)
1.8	0.628(3)	0.015(5)	0.0056(6)
2	0.549(4)	0.042(3)	0.0142(5)
$n = 8$			
1.6	0.738(2)	0.00009(4)	0.0000075(6)
1.8	0.685(4)	0.0006(2)	0.000079(5)
2	0.629(5)	0.0032(3)	0.00044(6)
2.2	0.570(2)	0.00132(1)	0.0016(4)
2.4	0.503(3)	0.0342(2)	0.0045(5)
2.5	0.465(2)	0.044(1)	0.0068(6)
$n = 16$			
2	0.666(3)	0.00001(2)	0.0000011(7)
2.2	0.616(2)	0.0006(3)	0.000014(6)
2.4	0.563(3)	0.0029(4)	0.000098(5)
2.6	0.507(4)	0.007(4)	0.00043(4)
2.7	0.478(3)	0.0118(3)	0.0008(5)
2.8	0.446(5)	0.019(8)	0.0014(6)

In Table 1, the values for liquid and vapour densities in equilibrium are presented for $n = 1$, 2, 4, 8, and 16.

3.2. Chemical potential results

Chemical potentials were obtained by means of Widom's insertion method for chain lengths of 1, 2, and 4 up to reduced densities of 0.9; the values are reported in Table 2. For chain lengths 8 and 16, at high densities, Widom's method became impractical, and thus chemical potentials could be obtained with this method up to a reduced density of 0.3 only. Pressures were determined for all chain lengths up to a reduced density of 0.9 for several temperatures. The results can be found in Table 3.

Figure 5 shows a μ–p diagram (an example for $n = 4$), where there appear three regions: vapour, liquid, and unstable. It is a frequently expressed view that the unstable region predicted by most EOSs (within the so-called van der Waals loop) cannot be observed by computer simulations. Our simulation results show, however, that van

Table 2. Reduced residual chemical potential for flexible Lennard-Jones chains of length n.

ρ^*	μ^*_{res} insertion	μ^*_{res} integration
$n = 1$, $T^* = 1$		
0.1	−1.03	−1.02, −0.991[1]
0.2	−1.91	−1.87
0.3	−2.56	−2.51, −2.436[1]
0.4	−3.08	−3.02
0.5	−3.55	−3.48, −3.48[1]
0.6	−3.81	−3.75
0.7	−3.52	−3.45, −3.477[1]
0.8	−2.25	−2.21
0.9	0.37	0.35, 0.243[1]
$n = 2$, $T^* = 1.4$		
0.1	−1.53	−1.59
0.2	−2.84	−2.83
0.3	−3.83	−3.80
0.4	−4.64	−4.61
0.5	−5.34	−5.28
0.6	−5.52	−5.46
0.7	−4.52	−4.46
0.8	−1.43	−1.46
0.9	4.41	4.49, 4.52[1]
$n = 4$, $T^* = 1.8$		
0.1	−2.42	−2.37
0.2	−4.49	−4.42
0.3	−6.10	−6.08
0.4	−7.50	−7.39
0.5	−8.25	−8.13
0.6	−7.61	−7.49
0.7	−4.18	−4.11
0.8	3.64	3.66
0.9	17.32	17.86, 17.75[1]
$n = 8$, $T^* = 2.4$		
0.1	−3.33	−3.22
0.2	−6.31	−6.18
0.3	−8.53	−8.36
0.4		−9.42
0.5		−8.53
0.6		−3.96
0.7		6.91
0.8		27.26
0.9		61.15, 59.45[1]
$n = 16$, $T^* = 2.7$		
0.1	−5.59	−5.50
0.2	−10.57	−10.42
0.3	−13.90	−13.68
0.4		−14.35
0.5		−10.51
0.6		14.93
0.7		26.91
0.8		72.27
0.9		145.72, 142.2[1]

[1]Johnson EOS.

der Waals loops do appear, but as artefacts of the averaging procedures: in the unstable region, the molecules tend to segregate, and two phases form. Figures 6–8 show snapshots of the central portion of the simulation box for $n = 4$, $T^* = 1.8$ for the same scale length. Figure 6 represents a vapour state with $\rho = 0.01$, which corresponds to point

Table 3. Reduced pressure for flexible Lennard-Jones chains of length n.

$n = 1$			
	p^*		
ρ^*	$T^* = 0.8$	$T^* = 1$	$T^* = 1.2$
0.1	0.020(9)	0.051(1)	0.080(3)
0.2	−0.054(7)	0.023(7)	0.092(2)
0.3	−0.145(2)	−0.036(4)	0.072(2)
0.4	−0.242(6)	−0.114(7)	0.043(4)
0.5	−0.425(3)	−0.223(8)	0.031(2)
0.6	−0.665(4)	−0.268(3)	0.157(6)
0.7	−0.653(5)	0.038(2)	0.700(2)
0.8	0.056(9)	1.095(1)	2.050(1)
0.9	1.970(7)	3.433(3)	4.757(6)
$n = 2$			
	p^*		
ρ^*	$T^* = 1.2$	$T^* = 1.4$	$T^* = 1.6$
0.1	0.016(7)	0.033(3)	0.049(4)
0.2	−0.030(2)	0.010(9)	0.047(3)
0.3	−0.102(9)	−0.042(1)	0.019(2)
0.4	−0.200(1)	−0.114(7)	−0.016(8)
0.5	−0.346(4)	−0.195(9)	−0.022(2)
0.6	−0.460(1)	−0.170(4)	0.134(2)
0.7	−0.262(8)	0.240(1)	0.733(1)
0.8	0.698(1)	1.467(2)	2.203(3)
0.9	3.043(3)	4.131(5)	5.162(5)
$n = 4$			
	p^*		
ρ^*	$T^* = 1.6$	$T^* = 1.8$	$T^* = 2$
0.1	0.007(2)	0.016(3)	0.026(3)
0.2	−0.039(4)	−0.015(3)	0.008(6)
0.3	−0.115(8)	−0.074(9)	−0.032(8)
0.4	−0.217(3)	−0.145(2)	−0.067(3)
0.5	−0.320(6)	−0.182(1)	−0.039(3)
0.6	−0.297(2)	−0.042(5)	0.212(6)
0.7	0.145(3)	0.571(4)	0.985(8)
0.8	1.464(2)	2.115(4)	2.741(3)
0.9	4.323(1)	5.251(5)	6.143(3)
$n = 8$			
	p^*		
ρ^*	$T^* = 2.2$	$T^* = 2.4$	$T^* = 2.6$
0.1	0.004(1)	0.010(5)	0.015(6)
0.2	−0.031(4)	−0.015(2)	0.001(6)
0.3	−0.087(7)	−0.053(6)	−0.018(4)
0.4	−0.135(8)	−0.068(1)	−0.001(7)
0.5	−0.108(9)	0.016(6)	0.140(3)
0.6	0.154(1)	0.372(8)	0.587(6)
0.7	0.956(9)	1.312(7)	1.656(5)
0.8	2.759(5)	3.302(2)	3.827(5)
0.9	6.232(7)	7.019(6)	7.780(3)

(*Continued*).

Table 3. (*Countinued*).

$n = 16$			
	p^*		
ρ^*	$T^* = 2.5$	$T^* = 2.7$	$T^* = 2.9$
0.1	−0.004(2)	−0.0003(2)	0.003(6)
0.2	−0.042(1)	−0.0293(6)	−0.016(7)
0.3	−0.094(7)	−0.0634(8)	−0.033(8)
0.4	−0.120(3)	−0.0595(2)	0.001(4)
0.5	−0.042(6)	0.0723(5)	0.185(5)
0.6	0.318(1)	0.5198(8)	0.717(2)
0.7	1.280(2)	1.6095(2)	1.929(4)
0.8	3.324(5)	3.8304(4)	4.322(7)
0.9	7.142(8)	7.8812(3)	8.598(6)

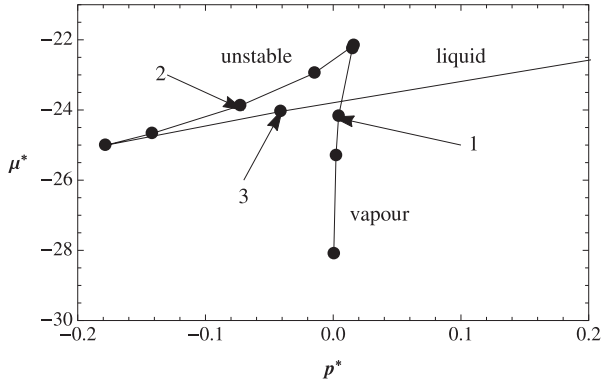

Figure 5. μ^*–p^* diagram for $n = 4$, $T^* = 1.8$.

1 in Figure 5, Figure 7 represents an unstable state (point 2), and Figure 8 represents a metastable liquid state (point 3). In the three situations, the same number of molecules is used, but we deliberately display the figures at the same length scale for better visualisation; this is why there appear to be fewer molecules in the vapour phase (Figure 6).

The segregation of the molecules in the unstable region is evident. Why is then a van der Waals loop observed? As pointed out by Yamamoto *et al*. [21,22], the summation in Equation (11), when carried out over all molecules, includes contributions from the liquid and vapour phase indistinctively including the interfacial region; summations confined to the liquid or vapour regions only would have yielded the equilibrium pressure.

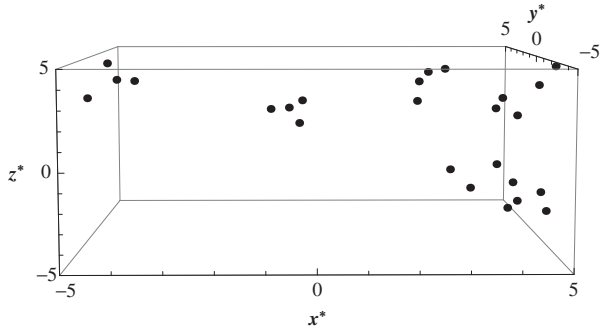

Figure 6. Snapshot of the centre of the simulation box ($n = 4$, $T^* = 1.8$, and $\rho^* = 0.01$).

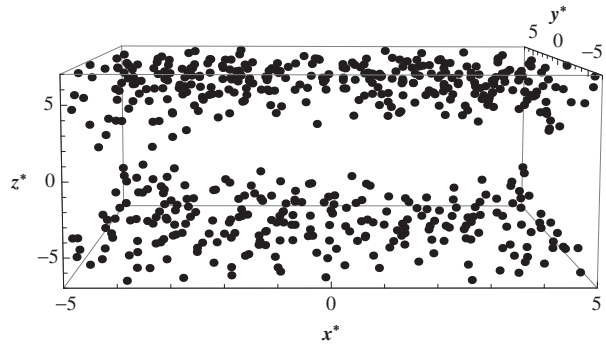

Figure 7. Snapshot of the centre of the simulation box ($n = 4$, $T^* = 1.8$, and $\rho^* = 0.3$).

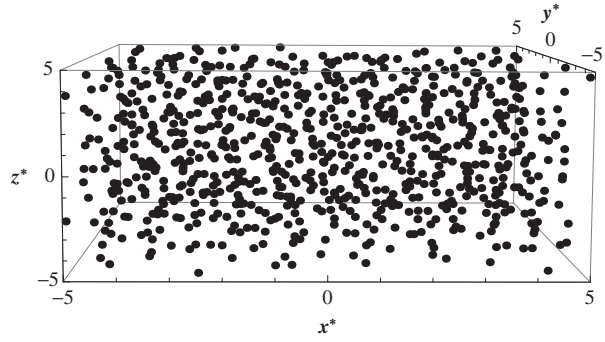

Figure 8. Snapshot of the centre of the simulation box ($n = 4$, $T^* = 1.8$, and $\rho^* = 0.8$).

Of particular interest is the intersection of the liquid and vapour branches in Figure 5, which corresponds to the vapour–liquid equilibrium. In order to determine the equilibrium, we fitted empirical functions to the branches and calculated their intersection. As $\partial\mu/\partial p = V_m$, the molar volumes of the coexisting phases can be obtained from the slopes of the branches. Table 4 shows the orthobaric densities thus obtained and compares them with densities obtained from the hyperbolic-tangent fits (cf. Section 3.1).

Table 4. Comparison of orthobaric bulk densities. Method 1: density profiles fitted with a hyperbolic-tangent equation, method 2: intersection and slopes of chemical potential diagram.

		Method 1		Method 2	
n	T^*	ρ^*_{liq}	ρ^*_{vap}	ρ^*_{liq}	ρ^*_{vap}
1	1	0.03	0.694	0.029	0.689
2	1.4	0.026	0.677	0.027	0.678
4	1.8	0.015	0.628	0.014	0.627

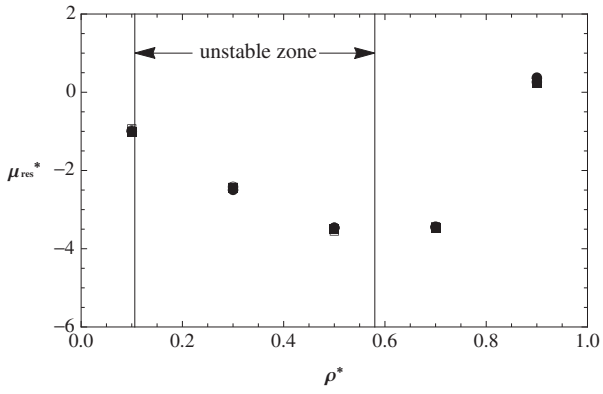

Figure 9. Reduced residual chemical potential as a function of reduced density for $n = 1$ at $T^* = 1$. •: MD simulation (this work), ○: EOS by Johnson *et al*. [7], ■: EOS by Mecke *et al*. [5], □: EOS by Quiñones-Cisneros *et al*. [23], and □: integration method, Equation (12).

Both methods reproduce the phase equilibrium of the systems quite well. Figure 9 ($n = 1$) compares some of the results with calculations from EOSs, which were carried out with the ThermoC program package [24].

4. Conclusions

Molecular dynamics simulations were performed for fluid systems consisting of flexible tangent-sphere LJ chain molecules with chain lengths between 1 and 16. The vapour–liquid equilibria of these fluids were determined either by simulating the evaporation of a liquid film, or from establishing the chemical potential equalities. The latter were obtained by means of Widom's insertion method or, where this became inefficient, with a thermodynamic integration method. The advantages of the second method rely on the fact that it is thermodynamically rigorous and that the evaluation of the chemical potentials is carried out over the whole simulation box. This procedure should, in principle, avoid uncertainties due to the interfacial width and should provide a more precise estimation of the equilibrium properties. The disadvantage is the additional effort required in the calculation of the chemical potentials using Widom's insertion method or the extra amount of simulations that is required for the integration procedure. In both cases, the orthobaric volume obtained with these methods agreed very well, and they also agreed with data from the literature, if available.

List of symbols

$\boldsymbol{F}_{ij}$	force exerted on particle i by particle j
h	Planck constant
k	spring constant
k_B	Boltzmann constant
n	number of atoms or sites in a chain
m_p	mass of one atom
N	total number of atoms
p	pressure
r	site–site separation
$r_{cut\text{-}off}$	cut-off distance
T	temperature
t	time
u_{bond}	bond potential
u_{LJ}	site–site interaction potential
V	volume of the simulation box
ΔU	change of the internal energy
ε	Lennard-Jones energy parameter
λ	de Broglie wavelength
μ	chemical potential
ρ	atomic number density
σ	Lennard-Jones site diameter

Funding

This work was carried out with the support of Consejo Nacional de Ciencia y Tecnología (CONACYT, México) PhD Scholarship 210692 to Patsy V. Ramírez-González and the Bilateral CONACYT (project 121214) – DFG (De 391/31-1).

References

[1] J.O. Hirschfelder, C.F. Curtiss, and R.B. Bird, *Molecular Theory of Gases and Liquids* (John Wiley and Sons, New York, 1954).
[2] J.J. Nicolas, K.E. Gubbins, W.B. Streett, and D.J. Tildesley, Mol. Phys. **37** (5), 1429–1454 (1979).
[3] F.H. Ree, J. Chem. Phys. **73** (10), 5401–5403 (1980).
[4] J. Kolafa and I. Nezbeda, Fluid Phase Equilib. **100**, 1 (1994).
[5] M. Mecke, A. Müller, J. Winkelmann, J. Vrabec, J. Fischer, R. Span, and W. Wagner, Int. J. Thermophys. **17** (2), 391–404 (1996).
[6] M. Lísal, K. Aim, M. Mecke, and J. Fischer, Int. J. Thermophys. **25** (1), 159 (2004).
[7] J.K. Johnson, E.A. Müller, and K.E. Gubbins, J. Phys. Chem. **98** (25), 6413–5419 (1994).
[8] F.J. Blas, L.G. MacDowell, E. de Miguel, and G. Jackson, J. Chem. Phys. **129** (14), 144703, 1–9 (2008).
[9] A. Trokhymchuk and J. Alejandre, J. Chem. Phys. **111** (18), 8510–8523 (1999).
[10] M.P. Allen and D.J. Tildesley, *Computer Simulation of Liquids* (Oxford University Press, Oxford, 1987).
[11] C.D. Holcomb, P. Clancy, and J.A. Zollweg, Mol. Phys. **78** (2), 437–459 (1993).
[12] A.R. Imre, G. Mayer, H. Házi, and T. Kraska, J. Chem. Phys. **128** (11), 114708, 1–11 (2008).
[13] G.A. Chapela, G. Saville, S.M. Thompson, and J.S. Rowlinson, J. Chem. Soc., Faraday Trans. 2 **73**, 1133 (1977).
[14] B. Widom, J. Chem. Phys. **39** (11), 2808–2812 (1963).
[15] J. Tobochnik, H. Gould, and J. Machta, Am. J. Phys. **73** (8), 708–716 (2005).
[16] G.C. Lynch and B.M. Pettitt, J. Chem. Phys. **107** (20), 8594–8610 (1997).
[17] C. Hoheisel and U. Deiters, Mol. Phys. **37** (1), 95–109 (1979).
[18] C. Reinsch, Numer. Math. **10** (3), 177–183 (1967).

[19] E. de Miguel and G. Jackson, J. Chem. Phys. **125** (16), 164109, 1–11 (2006).
[20] L.G. MacDowell and F.J. Blas, J. Chem. Phys. **131** (7), 074705, 1–10 (2009).
[21] R. Yamamoto, O. Kitao, and K. Nakanishi, Mol. Phys. **84** (4), 757–768 (1995).
[22] R. Yamamoto, H. Tanaka, K. Nakanishi, and X.C. Zeng, Chem. Phys. Lett. **231** (4–6), 401–406 (1994).
[23] S.E. Quiñones-Cisneros, U.K. Deiters, R. Rozas, and T. Kraska, J. Phys. Chem. B **113** (11), 3505–3511 (2009).
[24] U.K. Deiters, ThermoC project (University of Cologne, Cologne, 2006). <http://thermoc.uni-koeln.de/index.html>.